ASEG-PESA 2015
Geophysics and Geology together for Discovery
24th International Geophysical Conference and Exhibition
15–18 February 2015 Perth, Western Australia

3D geophysical model of the Glyde Basin, Northern Territory, based on curvatures derived from airborne gravity gradient data

Carlos Cevallos

CGG
69 Outram Street
West Perth
Western Australia 6005
carlos.cevallos@cgg.com

Peter Kovac

CGG
6100 Hillcroft
Houston
Texas 77081
peter.kovac@cgg.com

SUMMARY

This paper presents automatic 3D geophysical model generation based on equivalent pseudodepth slicing of the shape index of the equipotential surfaces derived from airborne gravity gradient data. The method is carried out in three steps. First, the pseudodepth slices of the vertical gravity gradient and the magnitude of the differential curvature components are generated. Second, the equivalent pseudodepth slices of the shape index are generated. Finally, 3D interpolation is carried out to obtain the final model.
The method is applied to FALCON airborne gravity gradiometer data from the Glyde Basin, Northern Territory and compared to an independently interpreted, integrated 3D geological Earth model.

Key words: Curvatures, gradients, gravity, shape index, Glyde Basin.

Introduction

Geophysical measurements yield a way of obtaining knowledge of the Earth's subsurface. They are normally presented as images or 2D surfaces and with the aid of theory and modelling they can be used to produce a 3D volume representation of a possible distribution of sources that generated the measured fields. Normally, at some part of this process two procedures are performed: a geological model made up from surfaces is manually constructed and mathematical inversion is used to validate it. Manual joining of interpreted surfaces is by far the most time-consuming part of building a 3D model; it requires an experienced geologist to construct complex geometries with digitisation tools. Each geologist generates a unique 3D model as the sources he interprets will fit his interpretation.

Curvature is a common theme in potential field interpretation, Phillips et al. (2007), Cooper and Cowan (2009), Cooper (2010) and Lee et al. (2013) have applied the concept of curvatures to estimate source location, depth and strike. The purpose of this paper is to show how to construct automatic 3D geophysical models based on curvatures of the equipotential surfaces defined by airborne gravity gradiometer (AGG) data without the need for manual work or inversion. These models will display gravity gradient information in a way that will aid interpretation of structural and lithological features, and estimation of the density distribution in the subsurface environment. The main goal is to assist the interpreter in the slowest part of interpreting AGG data: the construction of a 3D model. By quickly producing an initial unbiased 3D geophysical model the geologist will be able to see geometrical relations and will have surfaces at his disposal that he can then alter according to his interpretation. We will closely follow the curvature theory review from Cevallos et al (2013) and show the main results.

Theory

The curvatures of equipotential surfaces and their application to gravity gradiometry are well known in the study of differential geometry. Calculating the maximum and minimum curvatures that occur at unique orthogonal angles and averaging them yields a constant termed the mean curvature (Condi, 1999; Hofmann-Wellenhof and Moritz, 2006) (K_m):

$$K_m = (K_{max} + K_{min})/2 = -(1/2\Phi_z)\Phi_{zz} \quad (1)$$

where K_{max} and K_{min} are the maximum and minimum curvatures respectively. It is important to note a difference in the definition of the sign of the mean curvature according to different authors; in differential geometry, positive mean curvature is defined with concavity facing upwards; exploration geophysics uses the opposite definition (positive mean curvature is defined with concavity facing downwards) because is practical to associate positive density contrasts with positive curvature (Roberts, 2001).

The difference between the maximum and minimum curvatures is termed the differential curvature (Slotnick, 1932; Condi, 1999) (K_d):

$$K_d = K_{max} - K_{min} = (1/\Phi_z)[(\Phi_{xx} - \Phi_{yy})^2 + 4\Phi_{xy}^2]^{1/2}. \quad (2)$$

In differential geometry the most characteristic curvature of a surface is the Gaussian curvature defined as the product of the maximum and minimum curvatures. From equations 1 and 2 (Dransfield, 1994) (K_g):

$$K_g = K_{max}\,K_{min} = (1/\Phi_z)^2(\Phi_{xx}\,\Phi_{yy} - \Phi_{xy}^2). \quad (3)$$

As in the classical case of locating well-defined vertical faults using the zero contour of Φ_{zz} (Evjen, 1936), one would expect that along the boundary of a gravity source either the maximum or the minimum curvature would be zero and the zero contour of the Gaussian curvature should define the edges of sources.

Curvatures can be combined to define local shape, for example K_{max} and K_{min} can be combined to form a shape index (Koenderink and van Doorn, 1992; Roberts, 2001) (S_i):

$S_i = (2/\pi)\arctan[(K_{min} + K_{max})/(K_{min} - K_{max})]$. (4)

Substituting equations 1 and 2 in equation 4:

$S_i = (2/\pi)\arctan(-2K_m/K_d)$

$= (2/\pi)\arctan\{\Phi_{zz}/[(\Phi_{xx} - \Phi_{yy})^2 + 4\Phi_{xy}^2]^{1/2}\}$. (5)

As mentioned before, it is important to note what definition for the sign of mean curvature is used. This index defines local shape independently from scale, and can be used to classify the morphology of the equipotential surface. It can be presented as an image with nine colours with each colour representing different morphologies of the equipotential surface in terms of bowl, valley, flat, ridge and dome shapes (Roberts, 2001) with positive shape index values associated with positive density contrasts. The shape index of the equipotential surface enhances subtle trends and surface patterns that would be very difficult to identify in other images (Cevallos et al, 2013). If K_{max} or K_{min} are equal to zero, their substitution in Equation 4 yields:

$S_i = (2/\pi)\arctan(\pm 1) = \pm 1/2$. (6)

This result shows that the zero contour of the Gaussian curvature splits into the ± 1/2 contours of the Shape Index.

Spectral analysis (Spector and Grant, 1970; Gerard and Debeglia, 1975; Bhattacharyya, 1978) provides a technique for quantitative studies of magnetic or gravity data sets. Pseudodepth sections are derived from analysis of the log radially-averaged power spectrum of the data in the Fourier domain, which is a curve representing the amount of power in each wave number. Theoretically, the radially-averaged power spectrum can be broken up into a series of segments that approximate straight lines. Each of these segments can be related to the potential field signature of bodies at a particular depth, with the depth being proportional to the slope of the line. Once the straight-line segments have been identified, they are used to generate filters that are applied to the data in the wave number domain. Pseudodepth slices are then obtained by transforming the filtered Fourier spectra back into the space domain.

It can be shown that the power spectra of the curvature gradients Φ_{zz} and $[(\Phi_{xx} - \Phi_{yy})^2 + 4\Phi_{xy}^2]^{1/2}$ is identical (While et al, 2006; Dransfield and Christensen, 2013). This allows the following procedure: Spectral analysis is applied to both quantities to obtain their pseudodepth slices. Next, Equation 5 is used to calculate equivalent pseudodepth slices of the shape index. Finally, the equivalent pseudodepth slices of the shape index are interpolated to yield a 3D geophysical model.

Modeling

These ideas were tested using the synthetic model of Cevallos et al (2013). Two 1 km model cubes were assigned density contrasts of ±1.0 g/cm^3 respectively in a 2.67 g/cm^3 background density. The cubes are separated by 1 km and have a depth to top of 100 m. The shape index is presented in Figure 1A; note how positive shape index values are associated with positive density contrasts. Figures 1B, 1C, 1D, 1E and 1F show shape index pseudodepth slices at depths 125 m, 500 m, 1000 m and 2000 m respectively. They show that the shape index smoothness increases with depth and the dynamic range decreases with depth, that is, dome and bowl shape abundance diminishes with depth; this is a consequence of the equipotential surfaces becoming smoother if they are generated from deeper sources. They also show false high and low anomalies, false anomalies inside positions of bodies are a consequence of having an equipotential surface: if you have a high near a low (this model case) you will normally have an oscillatory behaviour in between the high and the low of the equipotential surface. All these behaviours of the shape index will occur independently of the actual behaviour of the density sources at depth and so it is extremely important to always keep in mind that curvatures and the shape index are directly linked to the equipotential surface and through it, indirectly to the density sources.

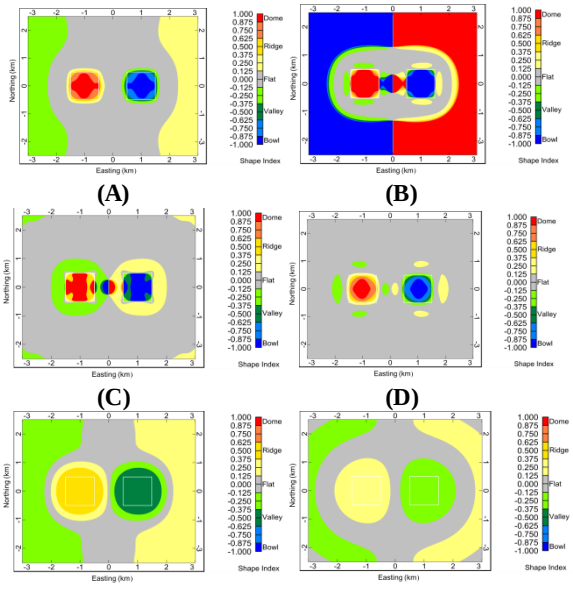

Figure 1. From Cevallos et al (2013). (A) Shape Index over the synthetic model cubes, shown by the white outlines (denser body on left); plus pseudodepth slices of the Shape Index over the synthetic model cubes, shown by the white outlines (denser body on left) at, (B) 125 m, (C) 250 m, (D) 500 m, (E) 1000 m and (F) 2000 m.

Application

The method was applied to AGG data in the Glyde Basin, Northern Territory (Figure 2). The 3D geophysical model was compared against a 3D Earth model from an independent geological interpretation in the southeast of the surveyed area (Kovac et al, 2014). This geological model was manually obtained and densities of lithologies were calculated using a 3D constrained inversion algorithm. Figures 3A, 3B, 3C and 3D show geological density model depth slices at depths 300 m, 500 m, 2500 m and 4700 m respectively.

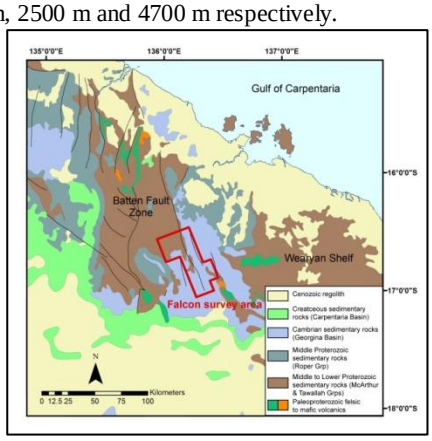

Figure 2. Location of the Glyde Basin survey area (red polygon) overlying geological map

Following the method proposed here, equivalent pseudodepth slices of the shape index were calculated. Then, the interpolated 3D geophysical model was produced using Geosoft's Oasis Montag 3D gridding algorithm with the kriging option and an exponential variogram model. Figures 4A, 4C and 4D show equivalent pseudodepth slices of the shape index at depths 270 m, 2500 m and 4660 m. Figure 4B shows an interpolated depth slice of the shape index at depth 500 m.

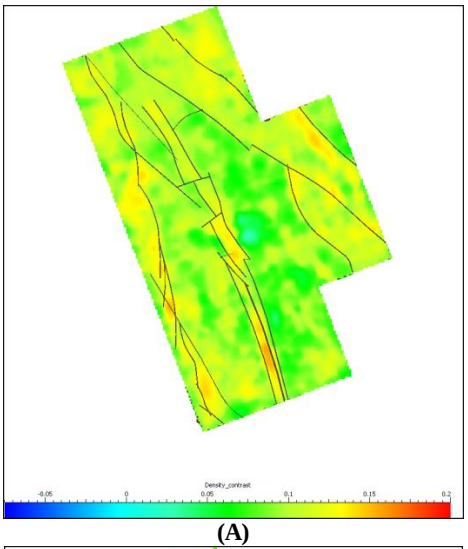

(A)

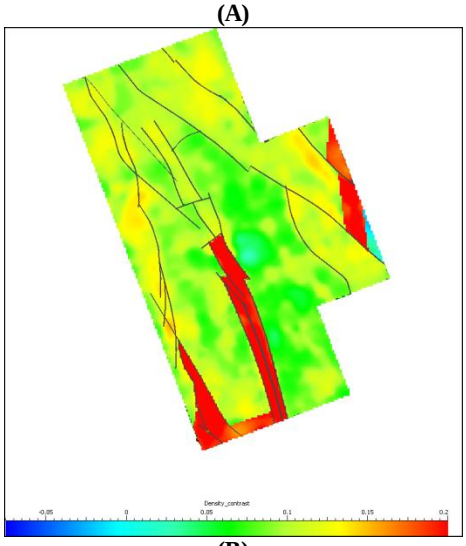

(B)

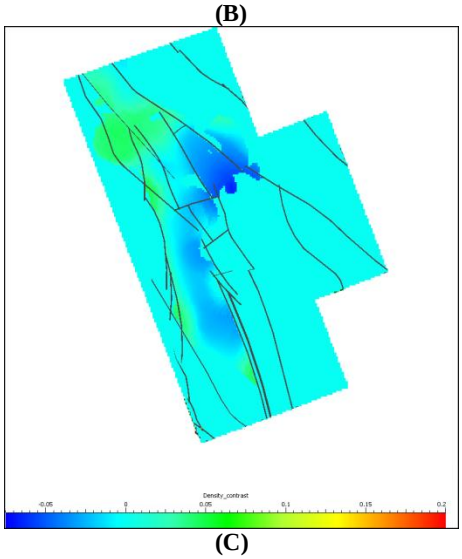

(C)

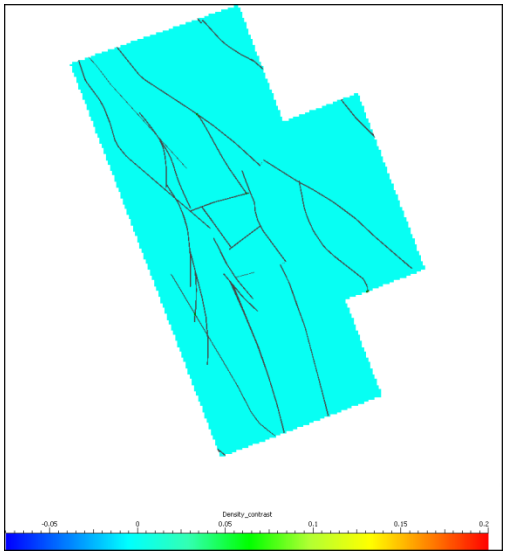

(D)

Figure 3. Depth slices of geological model at, (A) 300 m, (B) 500 m, (C) 2500 m, and (D) 4700 m. The colour bars represent density derived from the inversion process and ranges from –0.075 g/cm^3 to 0.2 g/cm^3. These densities are relative to the terrain correction density of 2.67 g/cm^3.

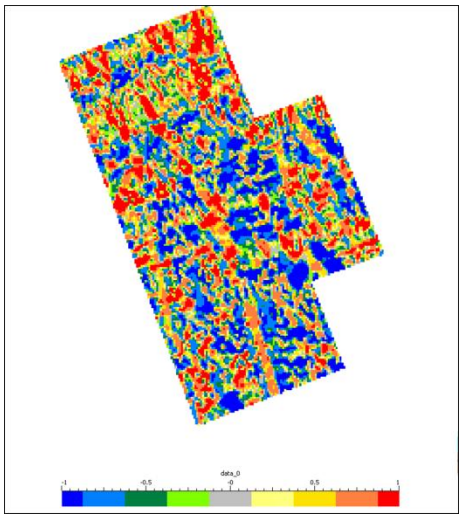

(A)

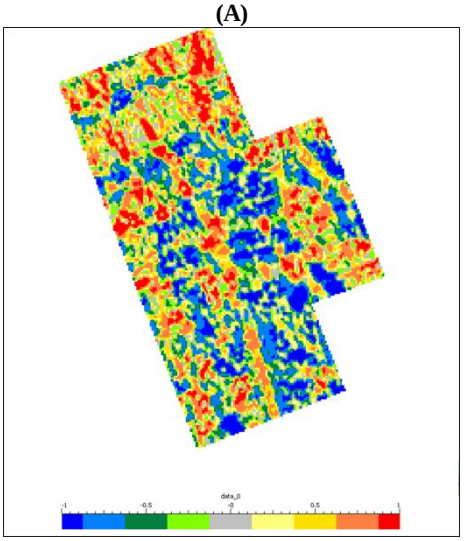

(B)

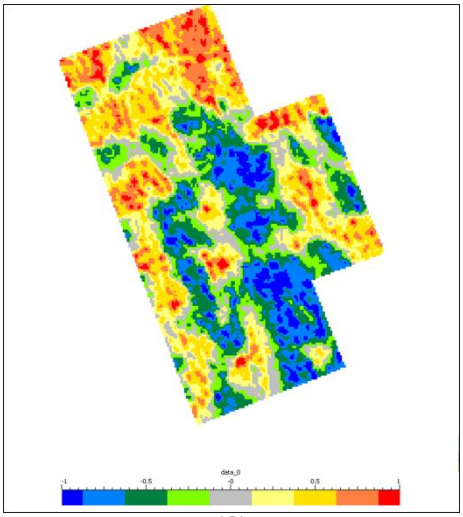

(C)

(D)

Figure 4. Equivalent pseudodepth slices of the shape index at; (A) 270 m, (C) 2500 m and (D) 4660 m. Interpolated depth slice of the shape index at (B) 500 m. The meaning of colours in the colour bars is the same as in Figure 1.

The 3D geological model exhibits abrupt density changes (Figures 3B and 3C) at boundaries defined by the interpretation. It also shows a homogenous bottom layer (Figure 3D), a necessity for inversion procedures. The 3D geophysical model exhibits two characteristics: one, it can generate well-defined surfaces at colour changes or isovalues; two, with depth the number of surfaces diminishes, that is, with depth some surfaces close or meld with each other.

Discussion

A 3D geophysical model based on curvatures of the equipotential surface provides us with direct and easily visualized information on the physics of the gravity gradiometry tensor. Curvature gradients relate the measured field directly to information of interest.

The 3D geophysical model generated from them is easy to understand and visualize. It should be noted that in spectral analysis there is always leakage between different pseudo-depth slices.

The application of the method shows that the geophysical model is more variable and smoother that the geological model, we have found this to be a general result. It is at the same time a strength and a weakness; its variations show some possibilities that may otherwise pass unnoticed but they could also add unnecessary detail or clutter at shallow depths.

Conclusions

The application of spectral analysis to curvatures gradients and the shape index allows the construction of a 3D geophysical model that immediately improves the understanding of location of mass and vertical edges, and provides an initial set of surfaces (independent of colour stretch) that can assist in the geological interpretation that is to follow.

Acknowledgements

The authors thank Armour Energy for permission to publish and Fabio Vergara for his assistance in producing the images.

References

Bhattacharyya, B. K., 1978, Computer modeling in gravity and magnetic interpretation: Geophysics, **43**, 5, 912–929.

Cevallos, C., P. Kovac, and S. J. Lowe, 2013, Application of curvatures to airborne gravity gradiometry data in oil exploration: Geophysics, **78**, 4, G81–G88.

Cooper, G. R. J., 2010, Enhancing Ridges in Potential Field Data: Exploration Geophysics **41**, 170–173.

Cooper, G. R. J., and D. R. Cowan, 2009, Terracing Potential Field Data: Geophysical Prospecting, **57**, 1067–1071.

Condi, F.J., 1999, Estimating subsurface structure through gravity and gravity gradiometry inversion: Ph.D thesis, Rice University.

Dransfield, M. H., 1994, Airborne gravity gradiometry: Ph.D. thesis, University of Western Australia.

Dransfield, M. H., and A. N. Christensen, 2013, Performance of airborne gravity gradiometers: The Leading Edge, **32**, 8 908–922.

Evjen, H. M., 1936, The place of the vertical gradient in gravitational interpretations: Geophysics **1**, 127–136.

Gerard, A., and N. Debeglia, 1975, Automatic three–dimensional modeling for the interpretation of gravity or magnetic anomalies: Geophysics, **40**, 6, 1014–1034.

Hofmann-Wellenhof, B., and H. Moritz, 2006, Physical geodesy 2nd ed.: Springer-Verlag Wien, 48–52.

Koenderink, J. J., and A. J. van Doorn, 1992, Surface shape and curvature scales: Image and Vision Computing, **10**, 557–564.

Kovac, P., L. Titus, C. Cevallos and J. Bluett, 2014, Exploring for hydrocarbon plays in the Glyde Basin, Northern Territory using FALCON®AGG data: APPEA Conference Proceedings **54**, Concurrent Session 21: New Horizons.

Lee, M.D., W. A. Morris, G. Leblanc, and J. Harris, 2013, Curvature analysis to differentiate magnetic sources for geologic mapping: Geophysical Prospecting, **61**, (S1), 572–585.

Phillips, J. D., R. O. Hansen, and R. J. Blakely, 2007, The use of curvature in potential field interpretation: Exploration Geophysics, **38**, 111–119.

Roberts, A., 2001, Curvature attributes and their application to 3D interpreted horizons: First Break, **19**, 85–100.

Slotnick, M. M., 1932, Curvature of equipotential surface: AAPG Bulletin **16**, 1250−1259.

Spector, A., and F. S. Grant, 1970, Statistical models for interpreting aeromagnetic data: Geophysics **35**, 293.